Role of Temperature in Partial Discharge Inception Voltage at Triple Junctions

Robert Szilágyi, Philippe Molinié, Michael J Kirkpatrick, E. Odic, Giacomo Galli, Philippe Dessante

Role of Temperature in Partial Discharge Inception Voltage at Triple Junctions

R. Szilágyi, Ph. Molinié, M. J. Kirkpatrick, E. Odic, G. Galli, Ph. Dessante

***Abstract*—In numerous industrial and electrical applications, within the zone near the junction between a metal conductor, a solid insulator and the surrounding gas, here called a triple junction, the local electric field created by the electric potential of the metal conductor may be enhanced due to the difference in the relative permittivity of the solid insulator and surrounding gas. This local field enhancement may facilitate the formation of partial electrical discharges (PD). Partial discharge activity can cause low-level damage as well as an accelerated aging which weakens the insulation system and then lead in the long term to complete breakdown. Therefore, in certain applications, such as in the aeronautical or nuclear sector, differences in temperature and gas pressure from the ambient case should be considered because of their influence on the partial discharge inception voltage (PDIV). The present work demonstrates a significant reduction in the PDIV in the case of a triple junction with alumina as the solid insulator when the system is heated to temperatures in the range of 300-400 °C. It is proposed that this effect is due to the increased permittivity of the alumina ceramic insulator at these temperatures, which leads to an increased enhancement of the local electric field at the triple junction. The proposed mechanism for local field enhancement is discussed considering, among others, permittivity measurements at elevated temperature.**

***Index Terms*—Partial discharge (PD), Paschen's law, nitrogen, triple junction electrodes, high temperature, aluminium oxide.**

I. Introduction

THE junction between a solid insulator, a solid conductor and the surrounding gas constitutes a triple junction (gas/metal/solid insulator), as illustrated in Fig. 1. In the case of overvoltages, the triple junction could be the starting point for electrical breakdown.

For applied voltages below the threshold for full dielectric breakdown, the intense electric field at the triple junction may nevertheless lead to the inception of partial electrical discharges initiated by gas ionisation phenomena. These partial discharges can lead to accelerated aging of the insulation system and cause low-level damage which may accumulate and gradually result in complete breakdown (dielectric breakdown and/or insulator flashover) [1], [2].

Ph. Molinié (philippe.molinie@centralesupelec.fr), R. Szilágyi, M. J. Kirkpatrick, E. Odic, G. Galli and Ph. Dessante are all with Université Paris-Saclay, CentraleSupélec, CNRS, Laboratoire de Génie Electrique et Electronique de Paris, 91192, Gif-sur-Yvette, France.

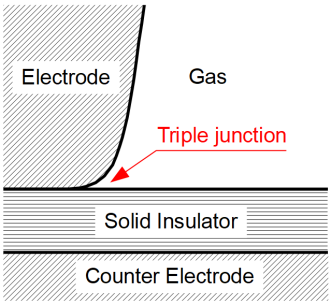

Fig. 1. Schema of a triple junction.

These triple junctions are often present in industrial applications where solid dielectrics are used to isolate high voltage conductors from other system components or from the ground as for example in Gas-Insulated Switchgears, Gas-Insulated Lines [3]–[5], or high voltage feedthroughs [6], [7]. In some circumstances, these solid insulators and the surrounding gas are exposed to environmental constraints in terms of pressure and temperature, as for example in the nuclear sector [8] and in the aeronautical sector [9]. In addition, the future increase in voltage for the purpose of the "More Electrical Aircraft" raises issues in regard to partial discharge activity which affects the reliability of the insulation system [10], [11].

Over the years, different studies have been published considering the influence of temperature and/or pressure on partial discharge activity [1], [9], [10] [12]–[14]. Other studies were made to examine partial discharge activity at triple junctions using different solid insulator materials, gas types and for varying gas pressure [1], [3], [15]. The main results of these studies show that discharge activity is facilitated with increased temperature and lowered pressure. Concerning triple junctions, the partial discharge activity depends on the material used as a solid insulator (the higher the permittivity, the easier it is to provoke partial discharges) as well as on the surrounding gas (nature and pressure).

Despite the interesting results presented in these studies, in most cases, the influence of different gas types or different solid insulator materials were examined whereas pressure and/or temperature remained at a constant level. However, applications in the nuclear sector are exposed to temperatures up to 500 *°C* [8] and in the aeronautical sector to pressures down to 100 *mbar* [16].

In the work reported in this paper, a broad range of temperature and pressures is considered, and specifically an

investigation is made regarding partial discharges at a circular triple junction at temperatures up to 400 °*C* with varying gas (N_2) pressure. Furthermore, the present work aims to come to a more detailed understanding of phenomena taking place at triple junctions under various conditions of pressure and temperature.

In section II, the theoretical background of Paschen's curve is presented. Section III describes the experimental arrangements. All experimental results are presented and discussed in section IV. Finally, section V gives a conclusion and prospects for future work.

II. Theoretical Background

A gas discharge can be initiated under the condition that seed electrons are accelerated by an external electric field to an energy superior to the ionisation energy of the bulk gas atoms or molecules. This leads to an electron avalanche. Sources of seed electrons can be cosmic rays, natural radioactivity of the earth, etc. These electron avalanches can lead in turn to gas discharge and breakdown.

Paschen's curve, named after the German physicist Friedrich Paschen who described it in 1889, characterises the conditions which lead to gas breakdown. More precisely, Paschen's curve gives the inception voltage for electrical breakdown in a gas as a function of the product of the gas pressure and the gas gap distance between two infinite planar electrodes. That means that the Paschen's curve is derived for the case of a homogeneous electric field. An analytical equation for Paschen's curve is given in (1) [17]:

$$V = \frac{A \cdot p \cdot d}{\ln(p \cdot d \cdot B) - \ln\left(\ln\left(1 + \frac{1}{\gamma}\right)\right)} \qquad (1)$$

where V is the breakdown voltage, p the gas pressure, d the distance between the electrodes, γ the secondary-electron-emission coefficient (an empirical constant representing the yield for the emission of secondary electrons – in this case limited to emission induced by positive ion bombardment of the cathode's surface which is typically taken to be in the range 10^{-4}-10^{-2}).

The constants A and B can be calculated according to (2) and (3):

$$A = \frac{\varepsilon_i \cdot \sigma}{k_B \cdot T} \qquad (2)$$

$$B = \frac{\sigma}{k_B \cdot T} \qquad (3)$$

where ε_i is the gas ionisation potential, σ the collision cross section for electron-gas ionisation, T the gas temperature and k_B the Boltzmann constant. It may be noted that in (1), the pressure parameter is always divided by a factor $k_B \cdot T$, indicating the fact that it is the gas density which is important to the physical principal behind the formation of an electrical discharge. Fig. 2 shows the experimental Paschen's curve [18] in nitrogen at 25 °*C* (the black curve was made using data from reference [18]

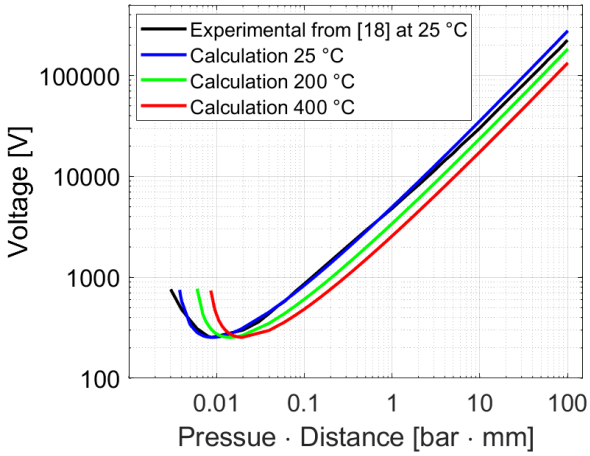

Fig. 2. Paschen's curves in nitrogen: experimental curve at 25 °*C* [18] and calculated curves for different temperatures (25 °*C*, 200 °*C*, 400 °*C*).

for different electrode materials, based on results from various experiments, for different electrode materials) as well as three calculated (1) Paschen's curves in the same gas for different temperatures (25 °*C*, 200 °*C* and 400 °*C*). As for all other gases, Paschen's curve for nitrogen exhibits a minimum. At ambient temperature, this minimum corresponds approximately to 254 *V* at $8.82 \cdot 10^{-3}$ *bar·mm*. The relative agreement between the experimental and calculated curves at 25 °*C* confirms that (1) reasonably describes the phenomenon. In the left-hand branch of the curve, the breakdown voltage increases very strongly due to a lack of sufficient gas molecules available for the development of electron avalanches. For relatively high values of $p \cdot d$ (right-hand branch of the curve), the breakdown voltage increases linearly due to a weaker electric field strength caused by increased distance between the electrodes and/or a reduced mean free path because of higher gas pressure. The influence of gas temperature on breakdown and therefore on Paschen's curve is usually treated by using the ideal gas law, see (4), as proposed by Dunbar *et al.* [19]. The basic idea of Dunbar was to adjust the data in the abscissa to reflect the fact that if the temperature changes at a given pressure, the gas density (and therefore mean free path for collisions) will also change accordingly. As a result of the Dunbar correction, the Paschen's curves are shifted to the right with increased temperature which leads to a decrease in breakdown voltage for given values of $p \cdot d$. In the model represented by (1-3), this adjustment of the data is implicit. This effect can also be described using the equation of the ideal gas law, see (4), of the free mean path, see (5), and of the electrical field strength, see (6), which is considered to be homogeneous near the triple junction:

$$N = \frac{p}{k_B \cdot T} \qquad (4)$$

$$\lambda = \frac{1}{\sigma \cdot N} \qquad (5)$$

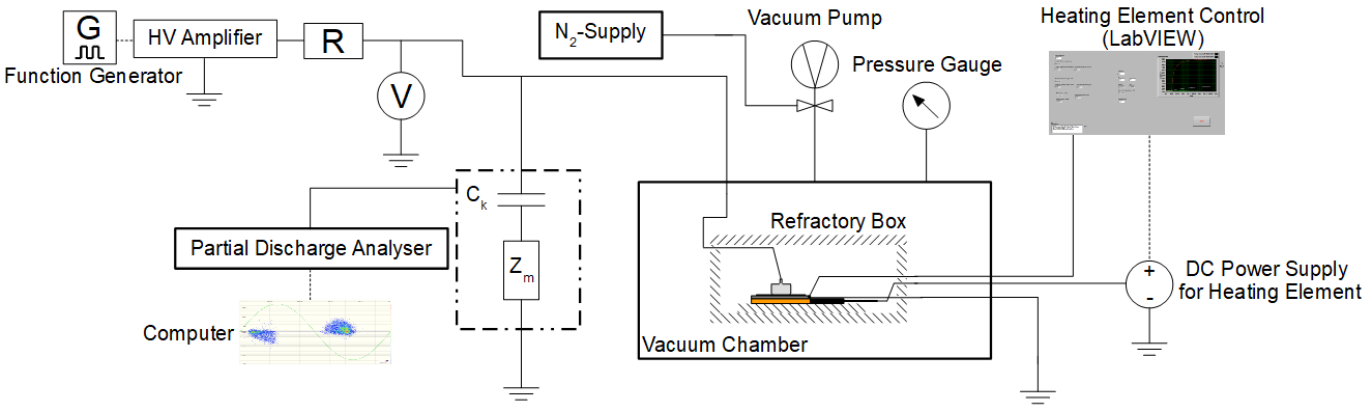

Fig. 4. Schematic showing of the experimental setup.

$$E = \frac{W}{q_e \cdot \lambda} \propto \frac{V}{d} \qquad (6)$$

where N is the gas density, λ the mean free path, E the electrical field strength, W the electrical work and q_e the elementary charge.

As can be seen in the above equations, an increase in temperature leads to a decrease in gas density which in turn leads to a greater value for the mean free path. Consequently, for a given gas ionisation potential, the electrical field strength and thus the voltage required for discharge inception decrease too.

Thus, by plotting the breakdown voltages of Fig. 2 as a function, not of the product $p \cdot d$, but as a function of the product $N \cdot d$, all the calculated curves merge whatever the temperature.

Finally, at this stage, it must be specified that in the case of a triple junction, the electric field is inhomogeneous and that consequently a deviation from the Paschen's curves will be observed.

III. Experimental Arrangements

A. Test Circuit

To test the triple junction at high temperature and different gas pressure / density, an experimental setup as pictured in Fig. 3 was constructed.

An aluminium oxide (99.7 % α-Al_2O_3 / ceramic α-alumina) disc (diameter of 50 *mm*, thickness of 1 *mm*) was used as dielectric test object. The ceramic α-alumina is an electrical insulator with a high dielectric strength which is used in many applications because of its stability at high temperature and good chemical resistance [20], [21]. All data presented in this work were obtained using a same 99.7 % α-Al_2O_3 ceramic disc, but other experiments using similar discs showed equivalent results.

As shown in Fig. 3, the aluminium oxide disc (4) was placed between a 30 *mm* diameter cylindrical tungsten electrode with Rogowski profile (3) and a 50 *mm* diameter stainless steel disc electrode (5). The surface roughness of the tungsten electrode was measured using an optical

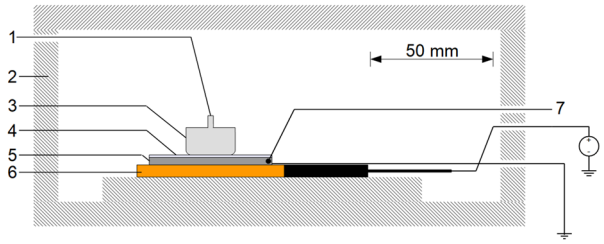

1 – HV-connection; 2 – Refractory box; 3 – Tungsten electrode; 4 – Aluminium oxide disc; 5 – Stainless steel electrode; 6 – Heating element; 7 – Thermocouple

Fig. 3. Schematic of the triple junction assembly including the heating plate inside the refractory box.

profilometry technique. An arithmetic average of profile height from the mean line (R_a) of 0.15 μm, with a quadratic mean of profile height considering deviations (valleys and peaks) from the mean line (R_q) of 0.2 μm were obtained. The tungsten electrode was connected (1) to a high voltage source and the stainless steel electrode was connected to ground. A ceramic (silicon nitride) heating element (6) was placed beneath the grounded electrode and was connected to a separate DC power supply (0-64 *V*, 0-6 *A*). This heating element could operate at temperatures up to 1000 °*C*, but in this work the maximum temperature used was 400 °*C*, as measured close to the triple junction. The temperature of the grounded electrode was measured by a thermocouple (7); this temperature was used as input for the control of the separate DC power supply. The triple junction assembly was placed in a refractory box (2) as shown in Fig. 3. This refractory box was constructed using porous aluminium oxide with a low thermal conductivity; its purpose was to homogenise the temperature around the triple junction and protect the outer wall of the vacuum chamber which was made of PMMA (poly(methyl methacrylate)). The refractory box, the vacuum chamber as well as the discharge analyser were placed in a Faraday Cage.

The refractory box with the triple junction assembly was part of the experimental setup which is depicted in Fig. 4.

As shown in Fig. 4, the high voltage power supply (Trek model 20/20C-HS), controlled via a function generator (in this work only used at 50 *Hz* sinusoidal) was placed in series with a 10 *MΩ* resistor to prevent any damage in case of breakdown. The electrical connection of the triple junction assembly between the vacuum chamber and the voltage source was made via a feedthrough. It may be noted that the feedthrough was insulated by PMMA, and therefore a second triple junction was present in the experiment. However, control experiments showed no discharge activity up to a voltage of 4.8 *kV* at ambient temperature and 4.5 *kV* when the temperature inside the refractory box was at 500 *°C*.

The AC voltage was measured using a high voltage probe (1 *V*:1000 *V*, 75 *MHz* bandwidth). To detect partial discharges, a commercial discharge analyser (OMICRON MPD 600) was used. This analyser was connected in parallel to the triple junction assembly via a 250 *pF* coupling capacitor and discharge pulses were detected according to IEC 60270 [22] using a frequency domain integration (centre frequency of 250 *kHz*, bandwidth of 300 *kHz*). To assure consistent measurements, voltage and charge calibrations of the discharge analyser were made before each experiment according to IEC 60270. For this purpose, a defined charge pulse (50 *pC*) was fed into the measuring circuit by a charge calibrator (OMICRON CAL 542) whereas the voltage was calibrated using the high voltage probe. The data produced by the discharge analyser were visualized using the software provided by Omicron. A partial discharge detection threshold value of 3 *pC* was achieved.

All the experiments were made inside a vacuum chamber using nitrogen. Nitrogen was chosen because of its similarity to air with regard to the Paschen's curve minimum and slope at high values of gas density and inter-electrode distance. The use of air was undesirable at high temperature because of oxidation of the metallic materials (electrodes of tungsten and stainless steel) inside the refractory box. A vacuum pump as well as a nitrogen supply were connected to the pressure chamber and the pressure was measured using a Pirani type sensor.

B. Temperature Control

The temperature of the gas close to the triple junction was an important parameter in this work. While the system was designed to have a temperature profile as homogeneous as possible, there remained nevertheless a temperature gradient from the heating element, extending out to the vacuum chamber. Experiments were made to determine the heat input necessary to obtain the desired temperature near the triple junction. These experiments consisted in the use of three thermocouples. The first thermocouple, also used in subsequent experiments and shown in Fig. 3, was placed within the grounded stainless steel electrode, itself in direct contact with the heating element. The other two thermocouples were placed i) wedged into the triple junction, and ii) in the gas approximately 2 *mm* from the triple junction. The heating element was controlled by a PI controller implemented within LabVIEW using the first thermocouple as input.

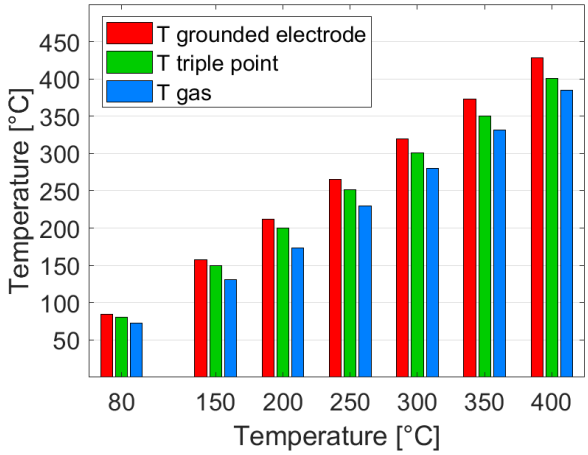

Fig. 5. Comparison of measured temperatures at the grounded electrode, at the triple junction, and its near proximity for nitrogen at atmospheric pressure.

The results of these experiments are described by the data shown in Fig. 5. The data in the figure were obtained at atmospheric pressure; additional experiments were also made for other pressure values. To reach the desired temperature at the triple junction, the setpoint required for the PI controller was therefore adjusted empirically: the value of the setpoint thus varied depending on both the pressure and temperature conditions.

Finally, a third thermocouple was used to measure the temperature in the gas at proximity to the triple junction (distance of ~2 *mm*) for selected junction temperature setpoints. The goal of this measurement was to estimate the temperature gradient and thereby its influence on the gas density near the triple junction from which discharges were expected to propagate. Fig. 5 shows the measured temperatures inside the grounded electrode above the heating element, at the triple junction, and in the proximity of the triple junction for atmospheric pressure, while using the previously determined setpoints. Depending on the emplacement of the thermocouples, the time to reach a stabilised temperature varied. Thus, it should be noted that all reported temperatures correspond to stabilised temperatures measured at least 1 *min* after reaching a stabilised gas temperature in the proximity of the triple junction which was the case 3 *min* after changing the setpoint. A stabilised temperature inside the grounded electrode was reached within 2 *min* and at the triple junction within 2 ½ *min*.

As shown in Fig. 5, the temperature inside the grounded electrode is the highest of the three measured temperatures. The temperature difference between the triple junction and the temperature measured about 2 *mm* away is about 8 *°C* for a setpoint of 80 *°C* and 15 *°C* for a setpoint of 400 *°C*. This

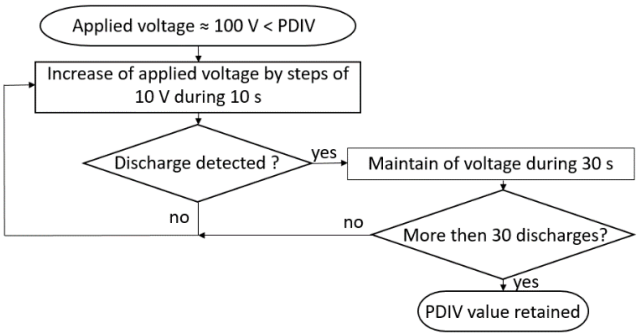

Fig. 6. Flowchart of the PDIV determination procedure.

difference in temperature leads only to a small difference in gas density of approximately $2.489 \cdot 10^{23}\ m^{-3}$ which is smaller than the measurement error for the density caused by the uncertainty of the pressure gauge according to the manufacturer.

It should be noted that observations may be found in the literature indicating that the discharge does not start at the exact location of the triple junction [1], [4], [23]. Consequently, in such a triple junction situation in presence of an inhomogeneous electrical field, the gas gap distance d is no longer fixed by the geometrical distance between the electrodes. A calculation of the discharge trajectory which varies with temperature and pressure in a range of a few hundred micrometres has been made in this work which validates the observations presented in literature. More details of this calculation will be presented in future work.

Hence, based on these observations, the gas densities at the triple junction and in its near proximity can considered to be homogeneous and a presentation of the obtained results only as function of pressure or gas density is relevant.

C. Experimental Procedure

After the installation of the test object inside the refractory box, the vacuum chamber was closed. To eliminate sources of uncertainty on the composition of the gas (for example outgassing of material with elevated temperature), the vacuum chamber was purged three times by pumping down to 3 *mbar* and then refilled with nitrogen (purity of 99.8 %) up to atmospheric pressure. This procedure was repeated each time the temperature was changed.

Each experiment was made beginning at the lowest temperature (ambient temperature), and then increasing up to the highest temperature (400 °*C*). For each temperature setpoint, the pressure was varied starting at the highest (atmospheric pressure) and then pumping down gas to reach lower gas pressure (50 *mbar*) / density values.

For given conditions of temperature and gas pressure / density, a standardised procedure was applied to detect the partial discharge inception voltage (PDIV). It should be noted that the voltage was first applied at the earliest 5 *min* after reaching a stabilised temperature in the gas in vicinity of the triple junction. Fig. 6 shows the flowchart of the PDIV determination procedure.

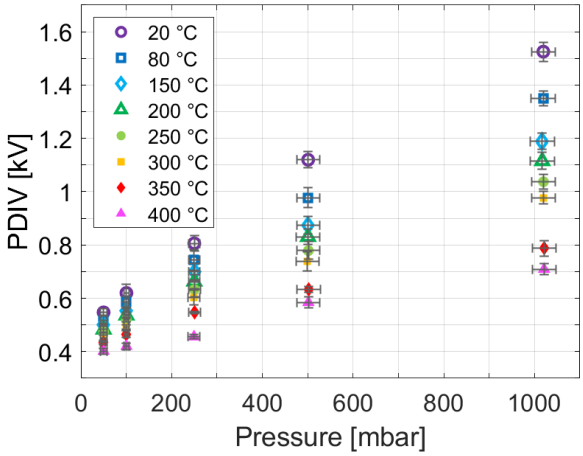

Fig. 7. PDIV as a function of pressure for different temperatures.

As shown in Fig. 6, the voltage applied to the test object was first adjusted approximately 100 *V* below the expected PDIV (which came from previous measurements). Then, the voltage was raised by steps of 10 *V* and maintained during 10 *s*. As long as no discharges were detected (detection threshold: 3 *pC*), the voltage was raised again by 10 *V*. Otherwise, the applied voltage was maintained for 30 *s*. If more than 30 discharge events were detected in this time interval, the PDIV value (AC voltage peak value) was retained. If not, the applied voltage was again raised by 10 *V*.

D. Measurement of Relative Permittivity

In addition to PDIV measurement for different temperatures and gas pressure / densities, the relative permittivity of the aluminium oxide disc was determined for different frequencies in the range from 20 *Hz* up to 1 *kHz* and for temperatures from ambient temperature up to 400 °*C* including a control measurement at ambient temperature after exposure to 400 °*C*. For this purpose, the same test circuit was used, and the measurement was made using a commercial LCR-meter (Wayne Kerr LCR Meter 4300) measuring the capacitance *C*. The relative permittivity was subsequently calculated using the thickness *e* of the aluminium oxide disc, the tungsten electrode surface *A* as well as the vacuum permittivity ε_0.

IV. Results And Discussion

A. PDIV for Triple Junctions: Dependence on Temperature as Function of Pressure

Fig. 7 shows the results for the PDIV in dependence on temperature as a function of pressure. Each data point was calculated from the average of 15 measurements (three repetitions of all temperatures and five repetitions for each

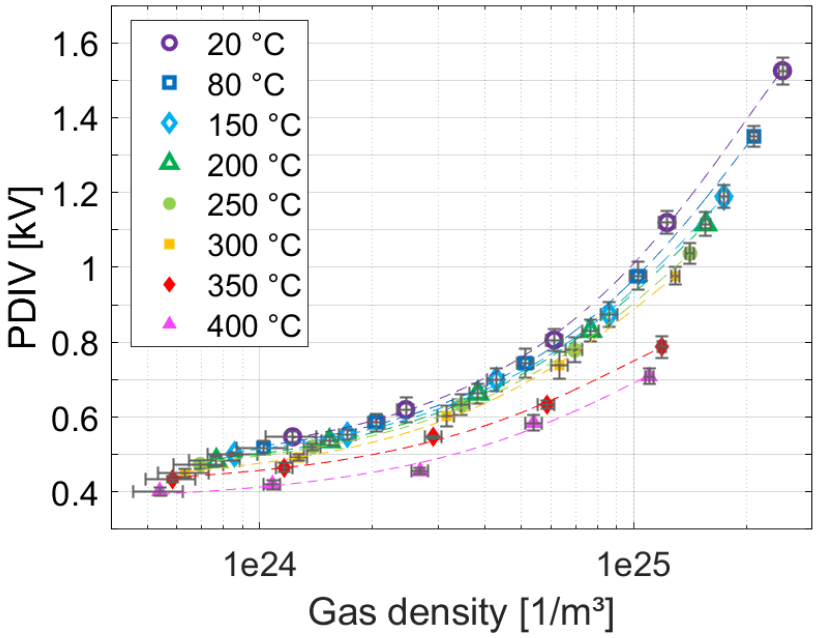

Fig. 8. PDIV as a function of gas density for different temperatures.

pressure). Error bars were calculated for a 1σ standard deviation.

Fig. 7 shows that, as expected, PDIV increases with pressure for all temperatures. Moreover, the obtained results show that an increase in temperature leads to a decrease in PDIV which is in accordance with the theory proposed by Dunbar. For instance, the PDIV difference between ambient temperature and 400 *°C* at atmospheric pressure amounts to 820 *V*.

B. PDIV for Triple Junctions: Dependence on Temperature as Function of Gas Density

Fig. 8 shows the results for the PDIV depending on temperature as a function of gas density. To make it easier to see the changes, all the points belonging to the same temperature experiments are connected with a trendline (second-degree polynomial).

Assuming that the gas density is homogeneous in the vicinity of the triple junction, it should be expected that all trendlines merge together when plotted as a function of gas density, according to calculations discussed in section II. However, as can be seen in Fig. 8, with increasing temperature up to 400 *°C*, all the curves are slightly below their precedent ones whereas a bigger gap between 300 *°C* and 350 *°C* can be observed. Consequently, for a given pressure, the increase in mean free path in the gas due to increase in temperature does not alone explain the decrease in PDIV.

Attention was then directed towards the role that the dielectric material (ceramic disc) could play on the PDIV as a function of temperature because studies showed that temperature may alter the properties such as the relative permittivity or volume conductivity of aluminium oxide

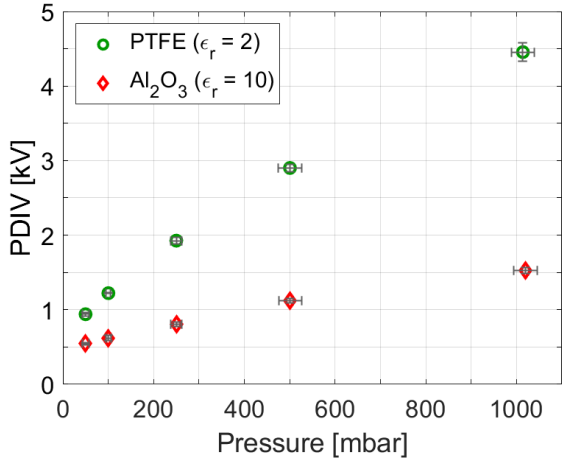

Fig. 9. PDIV as a function of pressure for two different materials (PTFE and aluminium oxide) in nitrogen at ambient temperature.

[15], [20].

C. Influence of Relative Permittivity Modification on PDIV

It should be noted that, in such an electrode arrangement, a change in the relative permittivity of the solid insulator leads to a change in PDIV. An approach to illustrate that is given by the comparison of the PDIV of two different insulating materials. More precisely, two geometrically identical (50 *mm* diameter, 1 *mm* thickness) discs of PTFE (ε_r = 2) and aluminum oxide (ε_r = 10) were compared at ambient temperature with respect to their PDIV. The

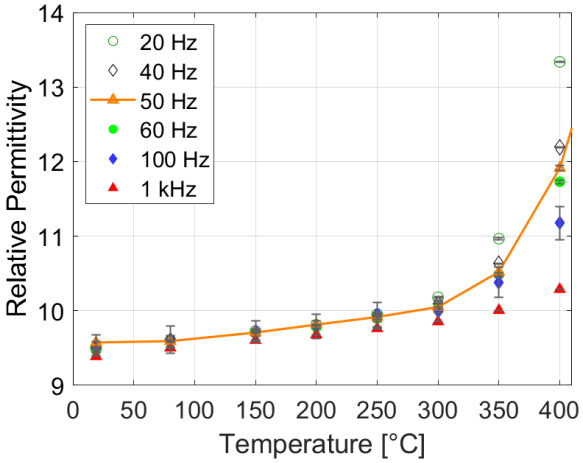

Fig. 10. Relative permittivity of 99,7 % aluminium oxide for different temperatures and frequencies. A solid line is highlighting the 50 *Hz* case.

experimental procedure was the same as described in section III. Fig. 9 shows the results.

As seen in Fig. 9, the PDIV for the PTFE disc is always higher than PDIV for the aluminium oxide disc. The reason for this is that a higher permittivity leads to increased polarisation of the insulator, which in turn leads to an increased electric field in the gas near the triple junction. Consequently, it can be stated (and calculated) that a higher relative permittivity leads to a lower PDIV.

In the case under investigation, a single insulating material was studied, but submitted to different temperatures. The relative permittivity of aluminium oxide is known to increase with temperature [20], [24]. To quantify this dependence, the relative permittivity of the aluminium oxide disc was measured in the temperature range under study for different frequencies, see Fig. 10.

For the experimental conditions presented in the work (frequency of 50 *Hz* and temperature range from ambient temperature up to 400 *°C*, cf. solid line in Fig. 10), the value of the relative permittivity varies between $\varepsilon_r \approx 9.6$ (ambient temperature) and $\varepsilon_r \approx 11.9$ (400 *°C*).

The higher relative permittivity at higher temperatures can be explained by the displacement of mobile charge carriers which is facilitated at high temperatures due to the increase in conductivity of the aluminium oxide. Since the charge quantity carried by conduction is approximately proportional to the duration of the applied voltage, the phenomenon of increase in relative permittivity is more distinct for lower frequencies. Hence, the results shown in Fig. 10 consolidate that the increase in relative permittivity at higher temperatures can indeed be explained by the increase in conductivity [20].

Thus, an increase in temperature leads to an increase in solid insulator relative permittivity, and consequently results, for a given gas density and electrode potential difference, in an increase in the local electric field strength near the triple junction. It is therefore logical that the PDIV

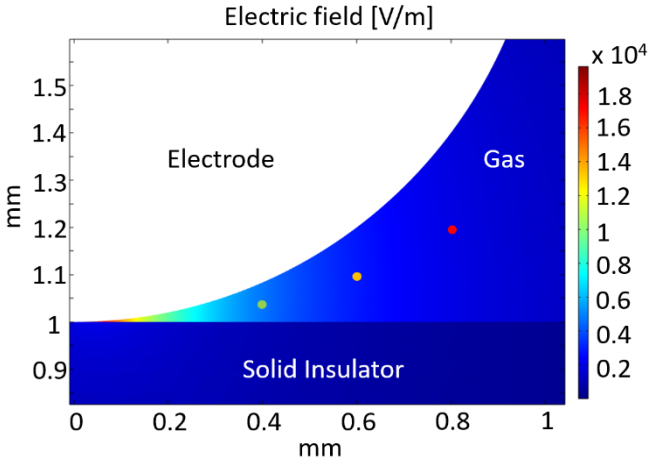

Fig. 11. Numerical simulation of the electric field near the triple junction for an applied voltage of 1 *V*. Further calculations were made for the coloured points.

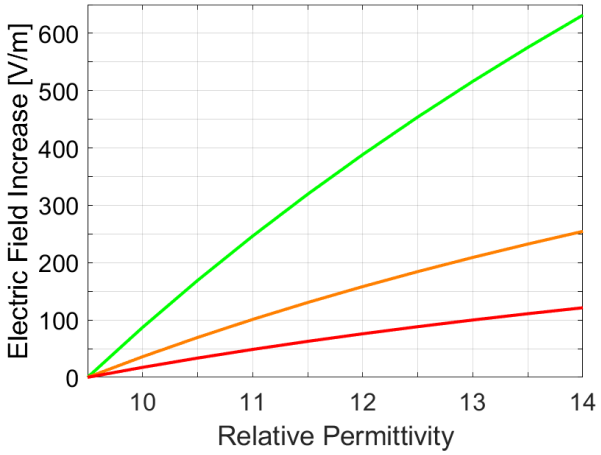

Fig. 12. Numerical calculation of the increase in electric field for different points in the gas near the triple junction in dependence of relative permittivity.

drops with temperature even more than may be expected simply due to the decrease in gas density.

This result can be supported by a numerical simulation of the electric field in the gas at proximity to the triple junction using finite element modelling (COMSOL Multiphysics). In Fig. 11, the electric field in vicinity of the triple junction for an applied voltage of 1 *V* is shown.

Additionally, a calculation of the variation of the local electric field in the gas as a function of the permittivity, varying from $\varepsilon_r = 9.5$ to $\varepsilon_r = 14$, was made for the three coloured points shown in Fig. 11 and is presented in Fig. 12.

As can be seen in Fig. 12, the higher the permittivity, the greater the increase in electric field with the increase being highest for the point closest to the triple junction. Despite the qualitative character of this numerical simulation, it can clearly be seen that an increase in relative permittivity leads to a reinforcement of the electric field in the gas near the

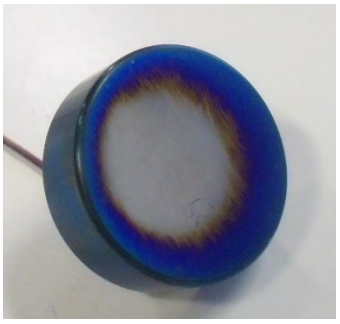

Fig. 13. Surface of the tungsten electrode after exposure to elevated temperatures (400 °C), protected (silvery colour) and oxidized (bluish colour) zones.

Table I

Comparison of relative permittivity and PDIV for a 96 % and 99,7 % aluminium oxide disc.

	96 %		99,7 %	
T [°C]	ε_r	PDIV [V]	ε_r	PDIV [V]
20	8,5	1745	9,6	1530
400	31	405	11,9	710

triple junction thus facilitating PD activity.

In this context, it should be noted that the effect of the increase in relative permittivity is even more important when an aluminium oxide with lower purity is used. Experiments have shown that the value of the relative permittivity using a 96 % aluminium oxide disc at 400 °C increases up to $\varepsilon_r \approx 31$. Hence, the PDIV at 400 °C for this specimen is about 305 V lower than for the specimen at 99.7 % purity, and the difference in PDIV between ambient temperature and 400 °C at atmospheric pressure for the 96 % purity specimen is about 1340 V compared to the previously mentioned 820 V for the 99.7 % purity alumina disc. Table I shows a comparison of the PDIV and relative permittivity values for both the 96 % and 99,7 % aluminium oxide disc at ambient temperature and 400 °C.

It should be noted that the same relative permittivity was measured during a control measurement at ambient temperature after exposure of the aluminium oxide disc to temperatures up to 400 °C. This demonstrates that exposure of the aluminium oxide disc to elevated temperatures did not irreversibly change its dielectric properties.

In Fig. 10, it may be observed that the increase in relative permittivity with temperature is more pronounced starting from 300 °C. This profile justifies the fact that in Fig. 8, the PDIV curve corresponding to 350 °C is clearly detached from that obtained at 300 °C. On the other hand, the difference between the curve at 350 °C and that at 400 °C should therefore be expected to have been even greater, given the profile of the curve of dependence of the relative permittivity with temperature. Oxidation of the surface of the tungsten electrode can be invoked as a mechanism to explain, at least partly, this discrepancy. Indeed, even though the vacuum chamber was purged with nitrogen three times before each experiment, it must be taken into account that

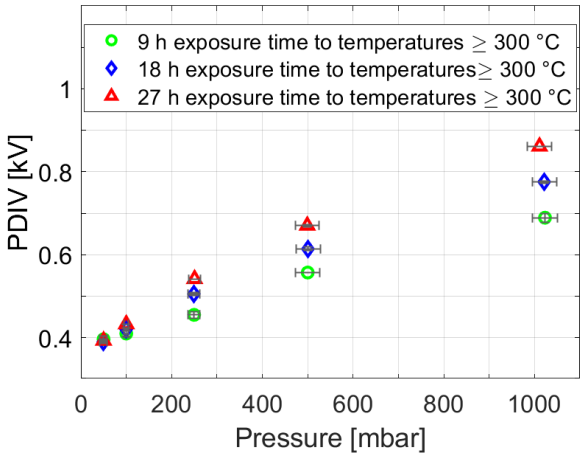

Fig. 14. PDIV at 400 °C as a function of nitrogen pressure for increasing exposure time of the tungsten electrode to temperatures above 300 °C.

Table II

Atomic concentration of tungsten and oxygen on the tungsten electrode surface for a cleaned/polished and an oxidised state.

	Cleaned/polished	Oxidised
Tungsten	84,2 %	45,3 %
Oxygen	15,8 %	54,7 %

some air leaked in during the experiments above 300 °C leading to a visible, bluish tungsten oxide layer on the surface of the tungsten electrode. This can be seen in Fig. 13 where a picture of the tungsten electrode with an oxidised (bluish colour) and a from oxidation protected (silvery colour) zone is shown.

Furthermore, an XPS-analysis measuring the atomic concentration of tungsten and oxygen to characterise the composition of the tungsten electrode surface for both the polished/cleaned and oxidised state was made. Table II shows the results.

The values in table II clearly indicate that the bluish coloured surface of the tungsten electrode shows a higher atomic concentration of oxygen than of tungsten whereas for the cleaned/polished electrode surface the tungsten predominates.

Finally, these results of the analysis support the hypothesis that it may be possible that the tungsten oxide layer has an influence on the secondary emission processes through the increase of the electron work function (from 4.5-5 eV to 6-7 eV) of the electrode material [25] [26], resulting in an increase in PDIV.

This effect is evidenced in Fig. 14 where the evolution of the PDIV for different pressures at 400 °C as a function of exposure time of the electrode to temperatures above 300 °C (350 °C and 400 °C) is shown.

It can be seen that with increasing exposure time to high temperature (≥ 300 °C), the PDIV measured at 400 °C tends to increase. From 9 h to 27 h, a rise of 170 V in PDIV was observed at atmospheric pressure.

Hence, the PDIV values presented in Fig. 7 and 8 for temperatures above 300 °*C* are potentially overestimated, even though the electrode surface was polished using a fine sandpaper (grain size of 22 μm) and then cleaned with alcohol using a precision wipe after each temperature cycle, so resulting in a 9 *h* maximum exposure time to temperature above 300 °*C*. It should be emphasised that this effect of oxidation is to increase the PDIV value whereas the main objective of this work is to explain the observed *reduction* in PDIV at higher temperatures, the proposed mechanism for which is the increased relative permittivity of the aluminium oxide insulator at higher temperatures, which results in higher local electric fields at a given applied voltage.

V. Conclusions

The present work reports on the effects of temperature and different gas pressure / densities on partial discharge inception voltage (PDIV) at triple junctions under 50 *Hz* AC high voltage conditions using a 99.7 % aluminium oxide disc.

It was observed that the PDIV decreases with increasing temperature and that the voltage drop becomes even more significant above temperatures of 300 °*C*. At atmospheric pressure, a drop of the value of PDIV of 820 *V* was measured when temperature was increased from ambient temperature up to 400 °*C*. When data are presented as a function not of pressure, but of gas density, an additional effect of temperature is observed. The net effect is a further lowering of PDIV values at higher temperatures in addition to what may be expected due simply to lower gas density. This additional effect is attributed to changes in the relative permittivity of alumina at higher temperatures, which results in increased electric fields near the triple junction for a given applied voltage. This idea was confirmed by dielectric measurements on aluminium oxide in the same temperature range, which highlighted the contribution of the insulating material to the PDIV drop for the highest temperatures through an increase of its relative permittivity.

In this context, it was noted that the effect of the increase in relative permittivity and hence the decrease in PDIV at 400 °*C* is even more important when using an aluminium oxide with lower purity (96 %) as an insulator.

All observed results are of interest for industrial applications where a triple junction is exposed to high temperature. Particularly the decrease in PDIV should be considered because partial discharges could lead to unexpected flashover of the insulating system.

Thus, future work will focus on the one hand on flashover conditions from a triple junction on ceramic insulators under high temperature conditions, and on the other hand on an in-depth study of the mechanisms and consequences of the oxidation of the electrode materials in the same conditions.

References

[1] C. Tran Duy *et al.*, 'Partial discharges at a triple junction metal/solid insulator/gas and simulation of inception voltage', *Journal of Electrostatics*, vol. 66, no. 5, pp. 319–327, May 2008, doi: 10.1016/j.elstat.2008.01.011.

[2] E. Odic, A. Goldman, M. Goldman, M. Dhainaut, and R. Dussart, 'Current distribution of AC surface discharges and associated chemistry', *Journal of Electrostatics*, vol. 64, no. 7, pp. 477–484, Jul. 2006, doi: 10.1016/j.elstat.2005.10.026.

[3] M. Michelarakis, P. Widger, A. Beroual, and A. (Manu) Haddad, 'Electrical Detection of Creeping Discharges over Insulator Surfaces in Atmospheric Gases under AC Voltage Application', *Energies*, vol. 12, no. 15, p. 2970, Aug. 2019, doi: 10.3390/en12152970.

[4] J.-H. Song, J.-Y. Kim, B.-Y. Seok, and Y.-C. Choi, 'Evaluation of discharge characteristics on the triple junction for development of the Gas-Insulated Switchgear', p. 5.

[5] M. S. Naidu, *Gas insulated substations*. New Delhi: I.K. International Pub. House, 2008.

[6] A. Simonin *et al.*, 'R&D around a photoneutralizer-based NBI system (Siphore) in view of a DEMO Tokamak steady state fusion reactor', *Nucl. Fusion*, vol. 55, no. 12, p. 123020, Nov. 2015, doi: 10.1088/0029-5515/55/12/123020.

[7] J. Jiang *et al.*, 'Partial Discharge Detection and Diagnosis of Transformer Bushing Based on UHF Method', *IEEE Sensors Journal*, vol. 21, no. 15, pp. 16798–16806, Aug. 2021, doi: 10.1109/JSEN.2021.3066809.

[8] G. Galli *et al.*, 'Characterization and Localization of Partial-Discharge-Induced Pulses in Fission Chambers Designed for Sodium-Cooled Fast Reactors', presented at the EPJ Web of Conferences, Jan. 2018, p. 03002. doi: 10.1051/epjconf/201817003002.

[9] D. L. Schweickart, D. F. Grosjean, D. G. Kasten, S. A. Sebo, and X. Liu, 'Low-Pressure Partial-Discharge Measurements: Monitoring the Insulation Integrity of Aircraft Power Wiring Systems', in *2008 IEEE International Power Modulators and High-Voltage Conference*, May 2008, pp. 568–571. doi: 10.1109/IPMC.2008.4743722.

[10] F. Koliatene, T. Lebey, J. P. Cambronne, and S. Dinculescu, 'Impact of the aeronautic environment on the Partial Discharges Ignition: A basic study', in *Conference Record of the 2008 IEEE International Symposium on Electrical Insulation*, Vancouver, BC: IEEE, Jun. 2008, pp. 603–606. doi: 10.1109/ELINSL.2008.4570404.

[11] B. Cella, T. Lebey, and C. Abadie, 'Partial discharges measurements at the constituents' level of aerospace power electronics converters', in *2015 IEEE Electrical Insulation Conference (EIC)*, Jun. 2015, pp. 274–277. doi: 10.1109/ICACACT.2014.7223587.

[12] E. Sili, J. P. Cambronne, N. Naude, and R. Khazaka, 'Polyimide lifetime under partial discharge aging: effects of temperature, pressure and humidity', *IEEE Trans. Dielect. Electr. Insul.*, vol. 20, no. 2, pp. 435–442, Apr. 2013, doi: 10.1109/TDEI.2013.6508745.
[13] Y. Li, Q. Zhang, Y. Zhao, T. Wang, G. Liu, and K. Wang, 'The influence of temperature on Partial Discharges and wormhole effect of oil-paper insulation under DC voltage', in *2017 IEEE Electrical Insulation Conference (EIC)*, Jun. 2017, pp. 100–103. doi: 10.1109/EIC.2017.8004704.
[14] R. H. Khawaja and T. R. Blackburn, 'Partial Discharge Patterns in Oil-Impregnated Paper and Pressboard Insulation at High Temperature', *Australasian Universities Power Engineering Conference*, p. 6, 2008.
[15] M.-A. Handala, 'Etude de la décharge de surface sous tension alternative 50 Hz - Effets sur une interface isolante air /solide', Thesis, Université Mouloud Mammeri, 2007. Accessed: Jan. 19, 2023. [Online]. Available: https://www.ummto.dz/dspace/handle/ummto/1259
[16] M. Karadjian, N. Imbert, C. Munier, M. Kirkpatrick, and E. Odic, 'Partial Discharge Detection in an Aeronautical Power Cable', in *2018 AIAA/IEEE Electric Aircraft Technologies Symposium*, Cincinnati, Ohio: American Institute of Aeronautics and Astronautics, Jul. 2018. doi: 10.2514/6.2018-5033.
[17] A. Küchler, *High Voltage Engineering: Fundamentals - Technology - Applications*. in VDI-Buch. Springer Vieweg, 2018. doi: 10.1007/978-3-642-11993-4.
[18] Dakin et al., 'Breakdown Of Gases In Uniform Fields Paschen Curves For Nitrogen, Air And Sulfur Hexafluoride', *Cigre 32*, p. 22, 1974.
[19] W. G. Dunbar and J. W. Seabrook, 'High Voltage Design Guide for Airborne Equipment', BOEING AEROSPACE CO SEATTLE WA, Jun. 1976. Accessed: Sep. 08, 2022. [Online]. Available: https://apps.dtic.mil/sti/citations/ADA029268
[20] L.-Y. Chen and G. W. Hunter, 'Temperature Dependent Dielectric Properties of Polycrystalline 96%Al_2O_3', *MRS Proc.*, vol. 833, p. G7.6, 2004, doi: 10.1557/PROC-833-G7.6.
[21] D. R. Lide, Ed., *CRC Handbook of Chemistry and Physics, 87th Edition*, 87th edition. Boca Raton, Fla.: CRC Press, 2006.
[22] 'IEC 60270:2000 | IEC Webstore'. https://webstore.iec.ch/publication/1247 (accessed May 14, 2021).
[23] M. Hara, T. Kurihara, S. Kozuru, J. Suehiro, and N. Hayashi, 'Estimation of partial discharge onset characteristics in gases around a triple junction', *Elect. Eng. Jpn.*, vol. 144, no. 1, pp. 1–11, Jul. 2003, doi: 10.1002/eej.10175.
[24] L.-Y. Chen, 'Dielectric Performance of a High Purity HTCC Alumina at High Temperatures - A Comparison Study with other Polycrystalline Alumina', *Additional Conferences (Device Packaging, HiTEC, HiTEN, & CICMT)*, vol. 2014, pp. 000271–000277, Jan. 2014, doi: 10.4071/HITEC-WP26.
[25] P. Reinicke, 'Herstellung und Untersuchung gesputterter transparenter Seilberelektroden für organische Solarzellen', Albert-Ludwigs-Universität, Freiburg, 2016.
[26] M. T. Greiner, L. Chai, M. G. Helander, W.-M. Tang, and Z.-H. Lu, 'Transition Metal Oxide Work Functions: The Influence of Cation Oxidation State and Oxygen Vacancies', *Advanced Functional Materials*, vol. 22, no. 21, pp. 4557–4568, 2012, doi: 10.1002/adfm.201200615.